Antihyperon Production in Antiproton-Proton Reactions at 3.7 BeV/c

C. BALTAY,† J. SANDWEISS,‡ AND H. D. TAFT
Yale University, New Haven, Connecticut
AND
B. B. CULWICK, J. K. KOPP, R. I. LOUTTIT, R. P. SHUTT, A. M. THORNDIKE, AND M. S. WEBSTER
Brookhaven National Laboratory, Upton, New York
(Received 25 June 1965)

Results on the production of antihyperons in the reactions of 3.7 BeV/c antiprotons with protons are presented. Examples were observed of the production of the antiparticles of all the baryons with hypercharge 0 and 1, several of which had not been observed prior to this experiment. The mass and lifetime of the $\bar{\Lambda}$ and the lifetimes of the $\bar{\Sigma}^{\pm}$ were measured and are consistent with the corresponding quantities of the Λ and $\Sigma^{\pm}$, as required by *CPT* invariance. In the two-body $\Lambda\bar{\Lambda}$, $\Lambda\bar{\Sigma}^0$, $\bar{\Lambda}\Sigma^0$, and $\Sigma^+\bar{\Sigma}^-$ final states the antihyperons displayed a very sharply forward peaked angular distribution. The production of the three-body final states $Y\bar{Y}\pi$ and $\Lambda\bar{N}K$ or $\bar{\Lambda}N\bar{K}$ tend to proceed through the $Y\bar{Y}^*$ or $\bar{Y}Y^*$ intermediate states, where the Y^* is either the Y_1^* (1385), the Y_0^* (1405), or the Y_0^* (1520). The four-body $\Lambda\bar{\Lambda}\pi^+\pi^-$ final state is dominated by the pair production of the Y_1^* (1385) hyperon isobar.

I. INTRODUCTION

AN extensive study of the reactions of high-energy antiprotons with protons has been carried out. The antiprotons were produced by the Brookhaven AGS, purified by an electrostatically separated beam,[1] and their interactions with protons were photographed in the Brookhaven 20-in. liquid hydrogen bubble chamber. 50 000 photographs at an incident $\bar{p}$ momentum of 3.3 BeV/c and 250 000 photographs at 3.7 BeV/c, with an average of 14 antiproton tracks per picture, were used in this study. The purpose of this report is to present final results on hyperon and antihyperon production in the reactions at 3.7 BeV/c. The results at 3.3 BeV/c have been reported previously[2–4] and are not included here, with the exception of the hyperon production cross sections which are listed for comparison.

The purpose of the investigation, aside from the observation of the antiparticles of all the known baryons with hypercharge 0 and 1, was to gain detailed information about the reaction mechanisms in the processes in which hyperons or antihyperons are produced. Approximately one-third of the hyperons were produced in two-body $Y\bar{Y}$ (hyperon-antihyperon) final states, and a large fraction of the three- and four-body final states proceed via two-body $Y\bar{Y}^*$, $\bar{Y}Y^*$, or $Y^*\bar{Y}^*$ intermediate states, where the Y^* is either the $Y_1^*(1385)$, the $Y_0^*(1405)$, or the $Y_0^*(1520)$. These processes seem attractive for reaction mechanism studies since theoretical interpretation might be easier for two-body final states than for final states involving many particles.

II. EXPERIMENTAL PROCEDURES

The antiprotons used in this experiment were obtained from interactions of the primary proton beam of the Brookhaven AGS in a tungsten or aluminum target placed inside the AGS vacuum chamber. The secondary beam was restricted to a narrow ($\pm 1.5\%$) momentum band and the antiprotons were separated out by a beam transport system containing two stages of electrostatic particle separators. The details of this beam transport system have been published previously.[1] The high-purity antiproton beam was passed through the Brookhaven 20-in. liquid-hydrogen bubble chamber where reactions with protons were photographed. On the average the beam consisted of 14 antiprotons per AGS pulse.

The fraction of beam particles that were antiprotons was evaluated by a careful study of δ-ray spectra pro-

TABLE I. Characteristics of the antiproton exposure.

	Lower energy	Higher energy
Beam momentum	3.28 BeV/c	3.66 BeV/c
No. of photographs	~50 000	~250 000
No. of tracks/picture	14.2	13.0
Total $\bar{p}$ path in H_2	24.8×10^6 cm	128.0×10^6 cm
$\bar{p}$ purity of beam	$(97\pm1)\%$	$(94\pm1)\%$
No. of hyperon events	342	1766

* Research carried out under the auspices of the U. S. Atomic Energy Commission.
† Present address: Physics Department, Columbia University, New York, New York.
‡ Alfred P. Sloan Foundation Fellow.
[1] C. Baltay, H. N. Brown, J. Sandweiss, J. R. Sanford, M. S. Webster, and S. S. Yamamoto, Nucl. Instr. Methods **20**, 37 (1963). See also Chap. II of Ref. 4.
[2] C. Baltay, E. C. Fowler, J. Sandweiss, J. R. Sanford, H. D. Taft, B. B. Culwick, W. B. Fowler, J. K. Kopp, R. I. Louttit, R. P. Shutt, A. M. Thorndike, and M. S. Webster, *Proceedings of the 1962 International Conference on High Energy Physics at CERN* (CERN, Geneva, 1963), p. 233.
[3] C. Baltay, T. Ferbel, J. Sandweiss, H. D. Taft, B. B. Culwick, W. B. Fowler, M. Gailloud, J. K. Kopp, R. I. Louttit, T. W. Morris, J. R. Sanford, R. P. Shutt, D. L. Stonehill, R. Stump, A. M. Thorndike, M. S. Webster, W. J. Willis, A. H. Bachman, P. Baumel, and R. M. Lea, in *Proceedings of the International Conference at Stanford, 1963* (Stanford University Press, Stanford, 1964), p. 267.
[4] C. Baltay, doctoral dissertation, Yale University, 1963 (unpublished).

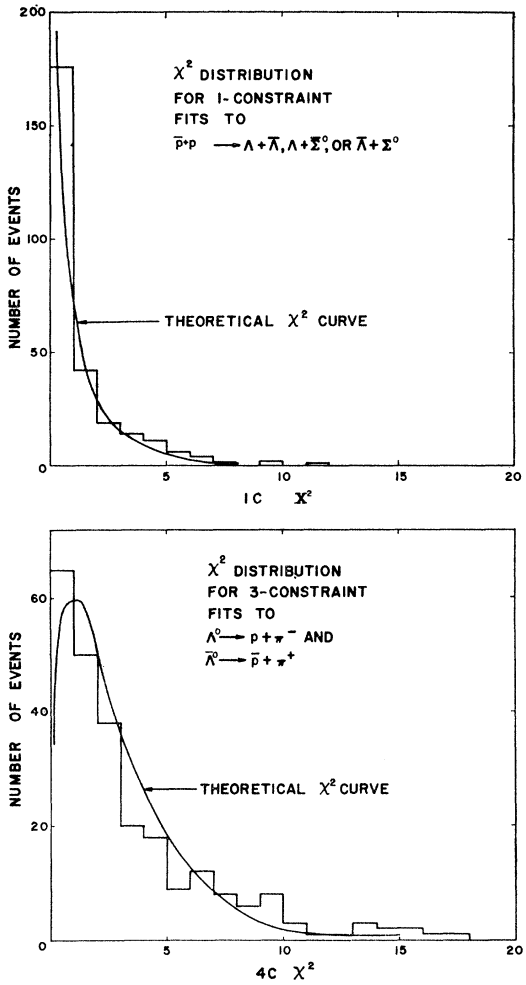

FIG. 1. Typical χ^2 distributions obtained in the kinematic fitting of events. The solid curves are the expected 1-constraint (top) and 3-constraint χ^2 distributions.

duced by beam-like tracks.[5] The best value of the beam momentum was taken to be the weighted average of the momenta of the antiprotons in 4-constraint kinematic fits, using a sample of 150 events involving one or two visible neutral strange particle decays. These and other properties of the exposure are listed in Table I.

The entire film was scanned twice for events with at least one visible neutral strange particle decay (vee) or at least one charged decay (kink). Vees which were obviously electron pairs, and kinks which were obviously proton scatters were discarded on the scanning table. The remaining events from both scans were then measured. The measuring process consisted of recording two-dimensional coordinates of points along the particle tracks in each of two stereoscopic views, using high-precision digitized measuring engines. From these measurements the three-dimensional event was reconstructed using IBM-7094 computer programs. The momenta and angles of all the tracks were computed, and these were used by the kinematic fitting programs to fit the event to the possible final state interpretations. In the present study, events were considered with 1 or 2 neutral decays with 0, 2, or 4 charged prongs at the production vertex, 1 or 2 charged decays with 2 or 4 charged prongs at the production vertex, and 1 or 2 charged decays with 1 or 2 neutral decays with 2 charged prongs at the vertex. The kinks or vees were usually first fitted as the decays of charged or neutral hyperons, and fits to the appropriate production hypotheses were attempted only if the required decay fits were satisfactorily achieved. Typical χ^2 distributions from these fits are shown in Fig. 1.

The above procedure produced 1766 events with at least one hyperon or antihyperon in the final state. The application of χ^2 criteria to the kinematic fits and the use of visual ionization information usually uniquely identified the charged particles in the final state of each event, and the neutrals with visible decays. In about one-half of the events, the missing neutrals, if any, were also uniquely identified. In the events where the missing neutral was not identified in this way, the missing mass spectra were used whenever possible to achieve an identification (see for example Fig. 2). The events where the χ^2 and ionization information did not uniquely identify the charged tracks were charged Σ pair events in which both sigmas decayed into charged pions, since

TABLE II. Hyperon production cross sections. Cross sections given are in μb for final state listed and its charge conjugate.

Final state	3.25 BeV/c	3.7 BeV/c
$\Lambda\bar{\Lambda}$	87±13	82± 8
$\Lambda\bar{\Sigma}^0$	56±11	69±10
$\Sigma^+\bar{\Sigma}^-$	36±13	44± 9
$\Sigma^-\bar{\Sigma}^+$	2_{-2}^{+8}	8± 4
$\Xi^-\bar{\Xi}^+$	4[b]	2[c]
$\Lambda\bar{\Lambda}+n\pi^0$ / $\Lambda\bar{\Sigma}^0+n\pi^0$	102±39	198±15
$\Lambda\bar{\Lambda}\pi^+\pi^-$	15± 6	27± 4
$\Lambda\bar{\Sigma}^0\pi^+\pi^-$	≤5	10± 3
$\Lambda\bar{\Lambda}\pi^+\pi^-\pi^0$ / $\Lambda\bar{\Sigma}^0\pi^+\pi^-\pi^0$	≤5	3± 1
$\Sigma^\pm\bar{\Sigma}^\mp\pi^0$	7[b]	12± 3
$\Sigma^+\bar{\Lambda}\pi^-$	54±15	70± 8
$\Sigma^-\bar{\Lambda}\pi^+$		24± 4
$\Sigma^+\bar{\Sigma}^0\pi^-$	12[c]	11± 3
$\Sigma^-\bar{\Sigma}^0\pi^+$		4± 2
$\Sigma^\pm\bar{\Lambda}\pi^\mp\pi^0$	6[a]	19± 3
$\Lambda\bar{n}K^0$	24±10	35± 7
$\Lambda\bar{p}K^+$		29± 5
$\Sigma^0\bar{p}K^+$		13± 4
$\Sigma^+\bar{p}K^0$		14± 4
$\Lambda\bar{n}\bar{K}\pi$	4[a]	9± 3
$\Xi^-\bar{\Xi}^0\pi^+$	≤5	3[c]
Total hyperon production	438±52	720±30

[a] Based on one event.
[b] Based on two events.
[c] Based on three events.

[5] T. Ferbel, A. Firestone, J. Sandweiss, H. D. Taft, M. Gailloud, T. W. Morris, A. H. Bachman, P. Baumel, and R. M. Lea, Phys. Rev. **137**, B1250 (1965).

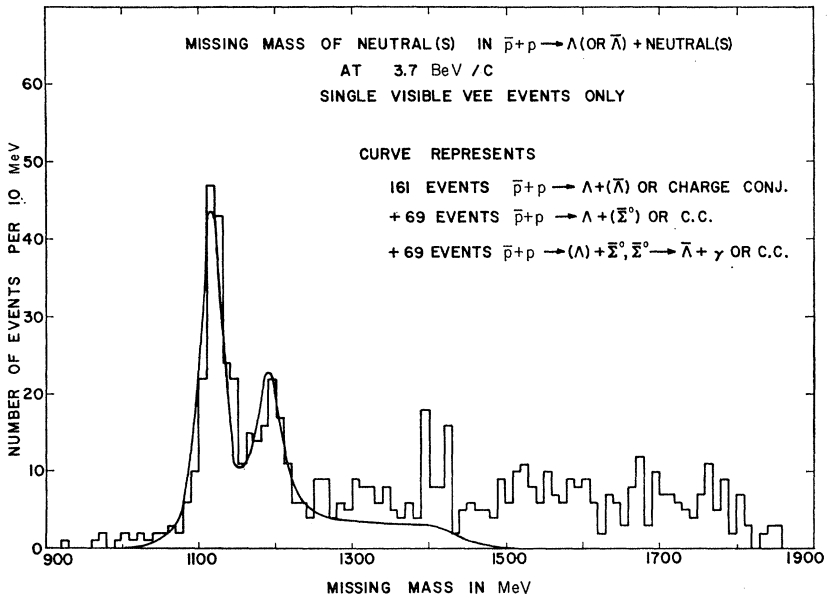

FIG. 2. Mass of neutral(s) in the reactions $\bar{p}+p \rightarrow \Lambda$ (or $\bar{\Lambda}$)+neutral(s). The curve represents the expected distribution, using the estimated resolution functions, for 161 events $\bar{p}+p \rightarrow \Lambda+(\bar{\Lambda})$ or charge conjugate, 69 events $\bar{p}+p \rightarrow \Lambda+(\bar{\Sigma}^0)$ or c.c., and 69 events $\bar{p}+p \rightarrow (\Lambda)+\bar{\Sigma}^0$, $\bar{\Sigma}^0 \rightarrow \bar{\Lambda}+\gamma$, or c.c. (Symbols in parentheses represent particles whose decay was undetected.)

the $\Sigma^+-\Sigma^-$ mass difference is not sufficient to differentiate between $\Sigma^+\bar{\Sigma}^-$ and $\bar{\Sigma}^+\Sigma^-$ final states. However, when the Σ or the $\bar{\Sigma}$ decayed into a p or $\bar{p}$, the event could be identified as a $\Sigma^+\bar{\Sigma}^-$ pair, and statistical arguments using the known decay branching ratios of the Σ^+ were used to estimate the $\Sigma^+\bar{\Sigma}^-$ and $\Sigma^-\bar{\Sigma}^+$ cross sections and angular distributions, as discussed in more detail in Sec. V.

The antiproton film used in this experiment was split into two equal parts. Events from one-half were scanned, measured, kinematically fitted and identified by the Brookhaven Bubble Chamber Group and events from the other half were processed at Yale University. The procedures used at the two laboratories differed in detail but were the same in essence. Identified hyperon events were then pooled and all further analysis was carried out on the combined BNL and Yale events together.

III. CROSS SECTIONS

An appreciable fraction of the events in which strange particles were produced escaped detection in this experiment either because the strange particles decayed outside the visible region of the bubble chamber, or the decay products were both neutral, or, in the case of a charged decay, the angle of the decay was so small that the kink was undetectable. The cross sections presented in Table II have been corrected for these losses by the use of an IBM-7094 computer program WEIGHT. For each observed event, WEIGHT computed the probability of detection of that event by a Monte Carlo method. In this calculation an average was taken over all the known parameters, such as the spatial distribution of the reactions in the chamber and the rotation of the events around the incident beam direction, but separate detection probabilities were computed for events with different momenta and production angles of the strange particles, the distribution of which was unknown *a priori*. A weight w_i was assigned to each event equal to the reciprocal of its detection probability. The total number of events of a certain kind was then calculated, using the formula

$$N=\sum_i w_i \pm [\sum_i (w_i)^2]^{1/2}. \quad (1)$$

The partial cross sections for the various hyperon production channels are shown in Table II. Final states which could not be unambiguously separated have been lumped together.

IV. ANTIHYPERONS OBSERVED AND THEIR PROPERTIES

The antiparticles of all the presently known strangeness -1 and -2 hyperons have been observed in this experiment: the $\bar{\Lambda}^0$, $\bar{\Sigma}^-$, $\bar{\Sigma}^0$, $\bar{\Sigma}^+$, $\bar{\Xi}^+$,[6] and the $\bar{\Xi}^0$.[7]

Approximately 300 visible $\bar{\Lambda}$ decays were observed; these were used to determine the mass and lifetime of the $\bar{\Lambda}$. The lifetimes of the $\bar{\Sigma}^-$ and the $\bar{\Sigma}^+$ were determined from 90 $\bar{\Sigma}^-$ and 25 $\bar{\Sigma}^+$ decays; (the $\bar{\Sigma}^+$'s come from the final states of the type $\pi^-\bar{\Sigma}^+\Lambda^0$, where there is no ambiguity with the Σ^+.) Since, in the decay of a charged Σ, there is always a neutral decay product, the masses of the $\bar{\Sigma}^\pm$ can not be determined well.

The best mass of the $\bar{\Lambda}$ was taken to be the weighted

[6] H. N. Brown, B. B. Culwick, W. B. Fowler, M. Gailloud, T. E. Kalogeropoulos, J. K. Kopp, R. M. Lea, R. I. Louttit, T. W. Morris, R. P. Shutt, A. M. Thorndike, M. S. Webster, C. Baltay, E. C. Fowler, J. Sandweiss, J. R. Sanford, and H. D. Taft, Phys. Rev. Letters 8, 255 (1962).

[7] C. Baltay, J. Sandweiss, H. D. Taft, B. B. Culwick, W. B. Fowler, J. K. Kopp, R. I. Louttit, J. R. Sanford, R. P. Shutt, D. L. Stonehill, R. Stump, A. M. Thorndike, and M. S. Webster, Phys. Rev. Letters 11, 165 (1963).

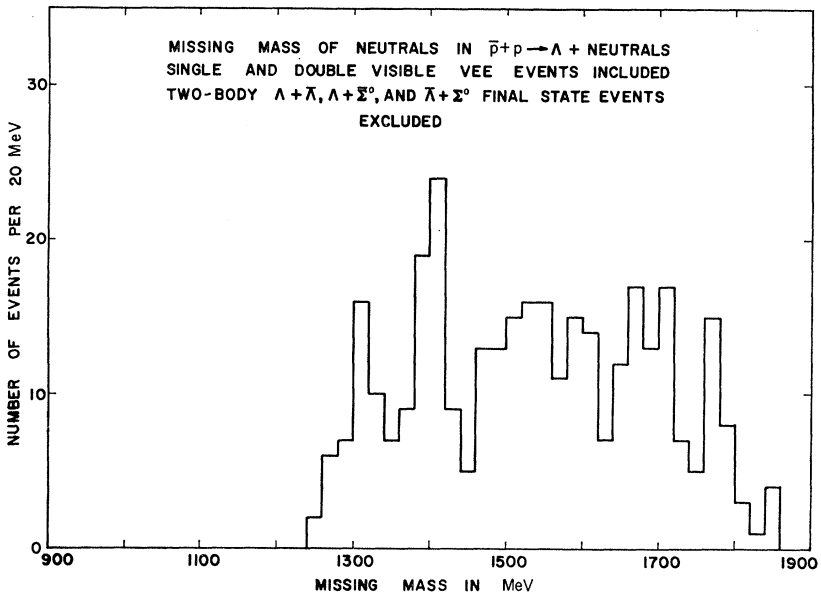

FIG. 3. Mass of neutrals in the reaction $\bar{p}+p \rightarrow \Lambda+$neutrals; two body $\Lambda+\bar{\Lambda}$, $\Lambda+\bar{\Sigma}^0$, and $\bar{\Lambda}+\Sigma^0$ events have been removed. The resolution in events where the observed decay was that of a $\bar{\Lambda}$ is much poorer than the resolution in events with visible Λ decays; therefore events with only a visible $\bar{\Lambda}$ decay have not been included in this distribution.

average of the mass calculated with its error for each $\bar{\Lambda}$ decay by the kinematic fitting programs. A maximum likelihood method was used to obtain the lifetimes of the $\bar{\Lambda}$ and $\bar{\Sigma}$'s. The likelihood function was written as

$$L(\tau)=\prod_i\left(\frac{1}{\tau}\right)\frac{e^{-(t_i/\tau)}}{e^{-({}_0t_i/\tau)}-e^{-({}_{\max}t_i/\tau)}}, \qquad (2)$$

where τ is the lifetime of the particle at rest, t_i is the observed proper time, ${}_0t_i$ is the minimum proper time consistent with observation, and ${}_{\max}t_i$ is the maximum proper time consistent with observation. Table III shows the results of the mass and lifetime calculations. The corresponding quantities were also computed for the Λ, Σ^+, and Σ^- to serve as a check on systematic errors.

The masses and lifetimes of the antiparticles are consistent with being equal to the masses and lifetimes of the corresponding particles, in agreement with *CPT* invariance.

V. TWO-BODY FINAL STATES

A. Neutral Two-Body Final States

Neutral two-body final states will be discussed first. The possible reactions are

$$\bar{p}+p \rightarrow \Lambda+\bar{\Lambda} \qquad (3a)$$

$$\rightarrow \Lambda+\bar{\Sigma}^0 \qquad (3b)$$

$$\Sigma^0+\bar{\Lambda} \qquad (3c)$$

$$\Sigma^0+\bar{\Sigma}^0 \qquad (3d)$$

$$\Xi^0+\bar{\Xi}^0. \qquad (3e)$$

The kinematic fitting programs did not try to fit the last two of these reactions [(3d) and (3e)]. The first three appeared in the bubble chamber as a disappearing incoming $\bar{p}$ track with one or two associated neutral Λ or $\bar{\Lambda}$ decays, since the Σ^0 or $\bar{\Sigma}^0$ decayed immediately into a Λ or $\bar{\Lambda}$ and a γ. When both the Λ and the $\bar{\Lambda}$ decayed visibly in the chamber, the kinematics usually identified the event as a $\Lambda\bar{\Lambda}$, a $\Lambda\bar{\Sigma}^0$, a $\bar{\Lambda}\Sigma^0$, or one of these with additional neutrals. 70% of the events in which either the Λ or the $\bar{\Lambda}$ was not visible were ambiguous between two or more of the above interpretations. The missing mass values were used to resolve these ambiguities. As can be seen in Fig. 2, there are two well-resolved peaks at the Λ^0 and Σ^0 masses.[8] $\Lambda\bar{\Sigma}^0$ or $\bar{\Lambda}\Sigma^0$ events in which the Λ or $\bar{\Lambda}$ is the decay product of the Σ^0 or $\bar{\Sigma}^0$ have a missing mass spectrum not peaked at the Σ^0 mass but spread out almost uniformly between 1130 and 1410 MeV. The resolution function for the missing mass was obtained from the double V events, and was

TABLE III. Masses and mean lifetimes of the Λ, $\bar{\Lambda}$, Σ^+, $\bar{\Sigma}^-$, Σ^-, and $\bar{\Sigma}^+$ hyperons.[a]

Particle	Mass (MeV)	Mean lifetime (10^{-10} sec)	No. of decays used for lifetime
Λ	1115.9±0.12	2.52±0.17	406
$\bar{\Lambda}$	1115.8±0.15	2.45±0.39	229
Σ^+	···	0.82±0.11	91
$\bar{\Sigma}^-$	···	0.88±0.15	90
Σ^-	···	$1.45_{-0.3}{}^{+0.6}$	19
$\bar{\Sigma}^+$	···	$1.95_{-0.5}{}^{+1.5}$	25

[a] The errors quoted are purely statistical. Any systematic errors, however, are believed to be the same for the particles as for their antiparticles.

[8] Both the Λ and the Σ^0 peaks in the missing mass distribution shown in Fig. 2 appear shifted to higher masses by about 10 MeV. The cause for this shift has been traced to the fact that the kinematic fitting programs used an incident beam momentum of 3.69±0.07 BeV/c. At the end of the analysis of the experiment, using a large sample of events, the correct beam momentum has been determined to be 3.66 BeV/c.

used to unfold the missing mass distribution of the single V events to obtain the production rates for the neutral two-body final states. The solid curve on Fig. 2 represents this fit.

Figure 3 shows the mass spectrum of the missing neutrals in the reactions $\bar{p}+p \rightarrow \Lambda+$neutrals. The two-body $\Lambda\bar{\Lambda}$, $\Lambda\bar{\Sigma}^0$, and $\bar{\Lambda}\Sigma^0$ events have been removed. Single V events where the visible V is a $\bar{\Lambda}$ decay have been excluded because these events have much poorer resolution then the events with a Λ decay visible (the $\bar{\Lambda}$'s have much higher momenta in the lab than the Λ's).

The distribution in the cosine of the antihyperon production angle in the $\bar{p}-p$ center-of-mass system for the $\Lambda\bar{\Lambda}$, $\Lambda\bar{\Sigma}^0$, and $\bar{\Lambda}\Sigma^0$ final states are shown in Fig. 4. These distributions have been corrected for detection losses and neutral decays of the Λ's or $\bar{\Lambda}$'s. From the unfolding of the missing mass distribution for these events (Fig. 2) it was estimated that the $\Lambda\bar{\Lambda}$ distribution has a 12% background of $\Lambda\bar{\Sigma}^0$ or $\bar{\Lambda}\Sigma^0$ events, and the $\Lambda\bar{\Sigma}^0$ or $\bar{\Lambda}\Sigma^0$ distribution has an 8% background of $\Lambda\bar{\Lambda}$ events. There is an additional 17% contamination in the $\Lambda\bar{\Sigma}^0$ or $\bar{\Lambda}\Sigma^0$ distribution which is made up of actual $\Lambda\bar{\Sigma}^0$ or $\bar{\Lambda}\Sigma^0$ events in which the observed Λ or $\bar{\Lambda}$ comes from the decay of the Σ^0 or $\bar{\Sigma}^0$, but which are misinterpreted as $\Lambda\bar{\Sigma}^0$ or $\bar{\Lambda}\Sigma^0$ events in which the observed Λ or $\bar{\Lambda}$ is the directly produced Λ or $\bar{\Lambda}$. The production angle of the antihyperon obtained from the incorrect fit for these events is in general not the true production angle. At the present energy, however, this error is usually smaller than 0.05 in $\cos\theta$.

The distributions for $\Lambda\bar{\Lambda}$ and $\Lambda\bar{\Sigma}^0$ or $\bar{\Lambda}\Sigma^0$ are very similar. In both, the antihyperons tend to keep the direction of the incident antiproton and the hyperons go backwards, in the direction of the incident proton, in the center-of-mass system. The sharp peaking of these distributions is very suggestive of some peripheral particle exchange mechanism. The system exchanged must have the quantum numbers $B=0$ and $S=1$, which implies a K, a $K^*(888)$, or some other combinations of a K meson and pions. The angular distributions are also presented as distributions in the four-momentum transfer squared in Figs. 5 and 6. The positions of the poles corresponding to the K meson and the $K^*(888)$, as well as the $K\pi$ branch cut, are indicated.

A number of theoretical attempts have been made to explain the sharpness of these angular distributions. Some good fits to the data have been achieved which indicate a strong predominance of $K^*(888)$ exchange.[9,10] For the details of these theoretical treatments of the $\bar{p}+p \rightarrow \Lambda+\bar{\Lambda}$ reaction the reader is referred to the literature.[9–14]

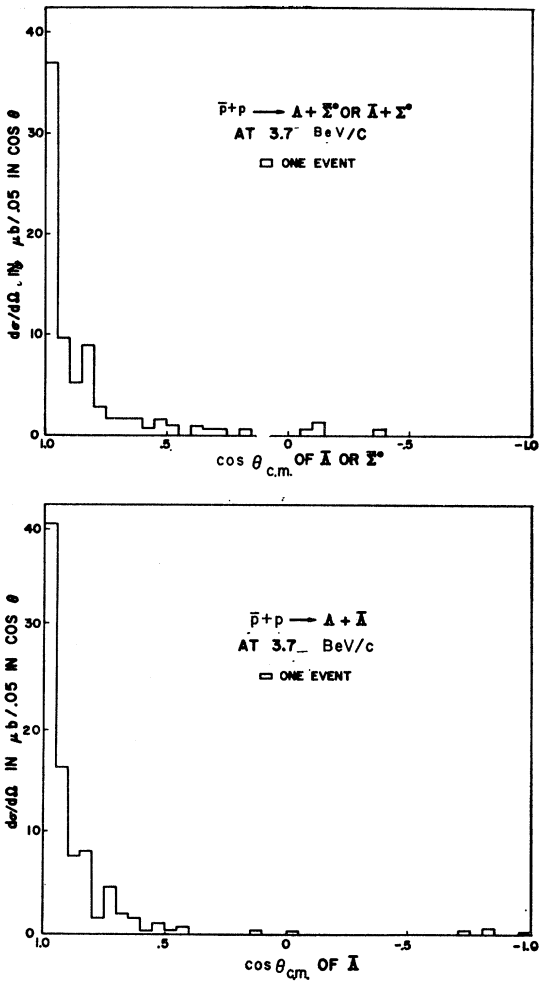

FIG. 4. Angular distributions of the $\bar{\Lambda}$ or $\bar{\Sigma}^0$ in the $\bar{p}p$ center-of-mass system for the reactions $\bar{p}+p \rightarrow \Lambda+\bar{\Lambda}$ and $\bar{p}+p \rightarrow \Lambda+\bar{\Sigma}^0$ or $\bar{\Lambda}+\Sigma^0$.

The polarization of the Λ and $\bar{\Lambda}$ particles in the $\bar{p}+p \rightarrow \Lambda+\bar{\Lambda}$ reaction has been measured making use of the parity-nonconserving decay of the lambdas. The angular distribution of the pion from the decay of the lambdas was fitted to

$$1+\alpha P\cos\theta,$$

where θ was the angle of the pion in the Λ c.m. system with respect to the normal to the $\Lambda-\bar{\Lambda}$ production plane, α is the parity-mixing parameter in lambda decay, and P is the average lambda polarization. Using the value[15] $\alpha=0.62\pm0.07$, the polarization was found to be consistent with zero:

$$P=0.09\pm0.18.$$

Because of the smallness of P, and the limited statistics, the comparison of α for the Λ and $\bar{\Lambda}$, which

[9] N. J. Sopkovich, doctoral dissertation, Carnegie Institute of Technology, 1962 (unpublished) and Nuovo Cimento **26**, 186 (1962).
[10] L. Durand, III and Y. T. Chiu, Phys. Rev. Letters **12**, 399 (1964).
[11] A. Dar, M. Kugler, Y. Dothan, and S. Nussinov, Phys. Rev. Letters **12**, 82 (1964).
[12] A. Dar, Phys. Rev. Letters **13**, 91 (1964).
[13] C. H. Chan, Phys. Rev. **133**, B431 (1964).
[14] L. Durand, III and Y. T. Chiu (to be published).
[15] J. W. Cronin and O. E. Overseth, International Conference on High Energy Physics (CERN, Geneva, 1962), p. 453.

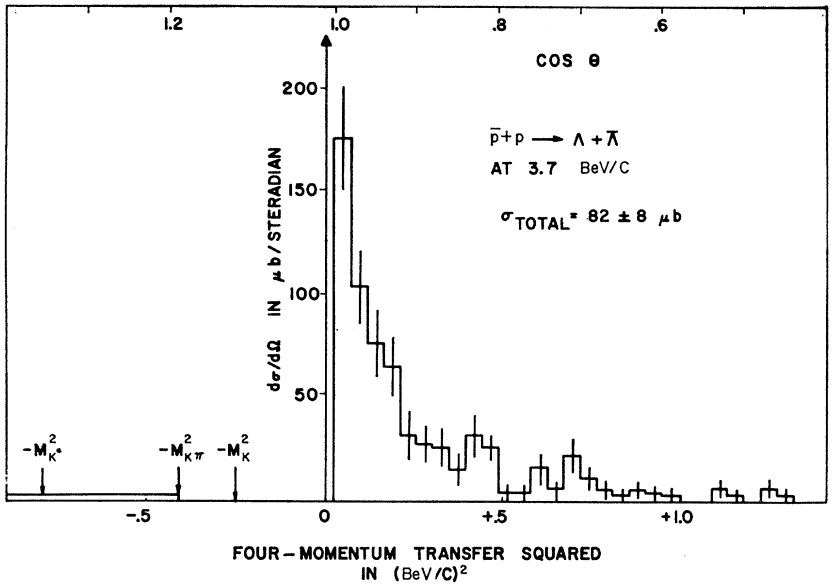

FIG. 5. Distribution in the square of the 4-momentum transfer in the reaction $\bar{p}+p \rightarrow \Lambda+\bar{\Lambda}$.

is a test of *CP* invariance, was not meaningful. The distributions for both Λ and $\bar{\Lambda}$ decays were combined in the above measurement of P.

The polarization of the hyperons in the $\bar{p}+p \rightarrow \Lambda+\bar{\Sigma}^0$ or $\bar{\Lambda}+\Sigma^0$ reactions was also consistent with zero.

B. Charged Two-Body Final States

The charged two-body final states observed were

$$\bar{p}+p \rightarrow \Sigma^+ + \bar{\Sigma}^- \quad (4a)$$

$$\rightarrow \Sigma^- + \bar{\Sigma}^+ \quad (4b)$$

$$\rightarrow \Xi^- + \bar{\Xi}^+. \quad (4c)$$

Kinematic fitting alone could not distinguish reactions (4a) and (4b) because of the small $\Sigma^+ - \Sigma^-$ mass difference. In those cases where one of the sigma decay products was a proton or an antiproton, the event could be identified as a $\Sigma^+\bar{\Sigma}^-$ pair. When the visible decay products were a π^+ and a π^-, however, the event remained ambiguous between reactions (4a) and (4b). Reaction (4c) was easily identified by kinematic fitting; in addition a Λ or $\bar{\Lambda}$ decay usually accompanied the events.

Table IV summarizes the decay modes of the observed $\Sigma\bar{\Sigma}$ pairs. The relative production rates of the $\Sigma^+\bar{\Sigma}^-$ and $\Sigma^-\bar{\Sigma}^+$ pairs can be estimated using the known decay branching ratios of the Σ^+ ($\Sigma^+ \rightarrow \pi^+ + n/\Sigma^+ \rightarrow$ all $= 0.475 \pm 0.017$).[16]

TABLE IV. Decay modes of the observed charged sigma pairs.

Class	Decay products of + sigma	Decay products of − sigma	No. of events observed
Unambiguous $\Sigma^+ + \bar{\Sigma}^-$	$p+\pi^0$	$\bar{p}+\pi^0$	11
	$p+\pi^0$	$\pi^- + \bar{n}$	34
	$\pi^+ + n$	$\bar{p}+\pi^0$	10
Ambiguous $\Sigma^\pm + \Sigma^\mp$	$\pi^+ + n$ or $\bar{n}$	$\pi^- + \bar{n}$ or n	62

Thus approximately $\frac{3}{4}$ of the $\Sigma^+\bar{\Sigma}^-$ pairs produced should be uniquely identified by one or both decays, and the number of $\Sigma^-\bar{\Sigma}^+$ decays is the number of ambiguous $\Sigma\bar{\Sigma}$ pairs minus $\frac{1}{3}$ the number of unique $\Sigma^+\bar{\Sigma}^-$ pairs. The same subtraction can be used to estimate the $\Sigma^+\bar{\Sigma}^-$ and the $\Sigma^-\bar{\Sigma}^+$ angular distributions. However, these subtractions will work only if the numbers of observed events are properly corrected for differences in detection efficiencies. The $\Sigma^+ \rightarrow p+\pi^0$ and $\bar{\Sigma}^- \rightarrow \bar{p}+\pi^0$ decays are detected with a much lower efficiency than the $\Sigma^\pm \rightarrow \pi^\pm + n$ and $\bar{\Sigma}^\pm \rightarrow \pi^\pm + \bar{n}$ decays because of large differences in characteristic decay angles and bubble density changes in the decays. The numbers of observed $\Sigma\bar{\Sigma}$ events were corrected for the detection losses mentioned above as well as for effects due to the different mean lives of the Σ^+ and Σ^-, utilizing an IVM-709 Monte Carlo program. The necessity of these corrections is evident from Table IV—the unweighted numbers observed for the three decay configurations of the uniquely identified $\Sigma^+\bar{\Sigma}^-$ pair are inconsistent with the known Σ^+ decay branching ratios.

After the proper corrections, the ratio of $\Sigma^+\bar{\Sigma}^-$ pairs to $\Sigma^-\bar{\Sigma}^+$ pairs was

$$R = \frac{\bar{p}+p \rightarrow \Sigma^+ + \bar{\Sigma}^-}{\bar{p}+p \rightarrow \Sigma^- + \bar{\Sigma}^+} = 5.5 \pm 2.0. \quad (5)$$

The distribution in the cosine of the production angle of the $\bar{\Sigma}$ in $\bar{p}+p \rightarrow \Sigma^+ + \bar{\Sigma}^-$ and $\bar{p}+p \rightarrow \Sigma^- + \bar{\Sigma}^+$, as obtained by the subtractions described above, are shown in Fig. 7. In the first reaction the $\bar{\Sigma}^-$ have a clear forward

[16] C. Y. Chang, J. Steinberger, and T. H. Tan, Bull. Am. Phys. Soc. **9**, 639 (1964).

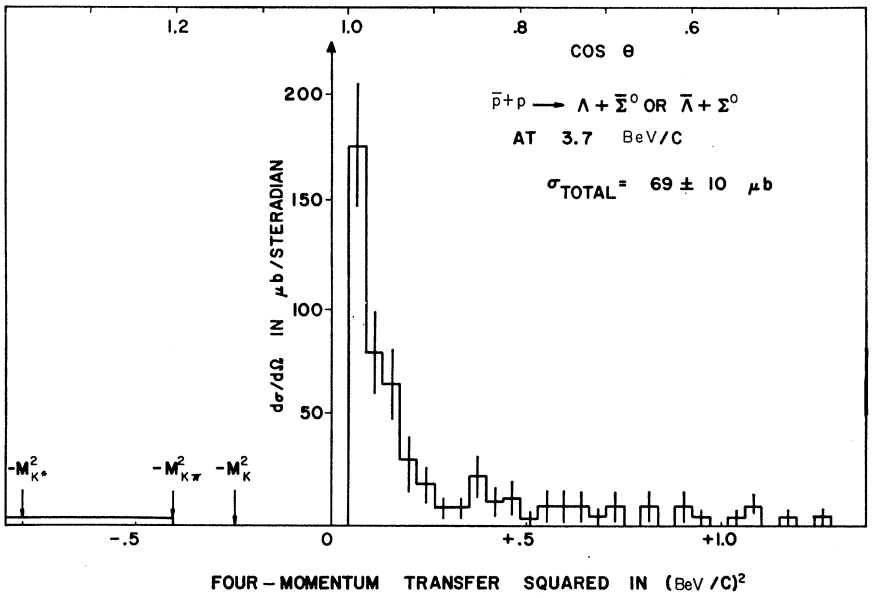

FIG. 6. Distribution in the square of the 4-momentum transfer in the reaction $\bar{p}+p \rightarrow \Lambda+\bar{\Sigma}^0$ or $\bar{\Lambda}+\Sigma^0$.

peak. For the second reaction the statistics are very poor, but the distribution is also consistent with a forward peaking of the $\bar{\Sigma}^+$.

Three events of the type $\bar{p}+p \rightarrow \Xi^-+\bar{\Xi}^+$ were observed in this experiment at 3.7 BeV/c incident $\bar{p}$ momentum, and two were found at 3.25 BeV/c. Three such events were also found in a similar experiment at CERN using 3.0 BeV/c antiprotons.[17] The data from these 8 events were combined to produce the production angular distribution of the $\bar{\Xi}^+$. Although the data are very meager, a tendency of the $\bar{\Xi}$ to be produced in the direction of the incoming $\bar{p}$ is apparent in Fig. 8.

C. Comparison with *SU3*

It is interesting to compare the production cross sections for the two-body processes $\bar{p}+p \rightarrow \bar{Y}+Y$ with the predictions of a simple octet exchange model based on *SU3*. Here Y stands for the hyperons Λ, Σ^0, or Σ^+. The production angular distributions in these two-body processes are sharply forward peaked (see Figs. 4 and 7) suggesting the dominance of a single K or $K^*(888)$ exchange mechanism. The fact that both the K and the K^* are members of the "8" representation leads to a model[18,19] for these reactions in which the amplitude associated with the "8" representation of *SU3* dominates over the amplitudes of the other representations connecting 8⊗8 with 8⊗8. There are, however, two independent octet amplitudes; the symmetric 8 (*D*-type coupling) and the antisymmetric 8 (*F*-type coupling). The ratios of the production rates for $\bar{p}+p \rightarrow \bar{Y}+Y$, as given by Tanaka,[19] are listed in Table V, along with the cross sections measured in this experiment. The experimental numbers are in reasonable agreement with the predictions for pure *F*-type coupling, but are in disagreement with the predictions for *D*-type coupling. However, Tanaka's calculations do not take into account absorptive effects in the incoming or outgoing channels. If such effects, which are likely to be present, were taken into account, the relative rates for *F*- and *D*-type coupling might be altered from the predictions listed in Table V.

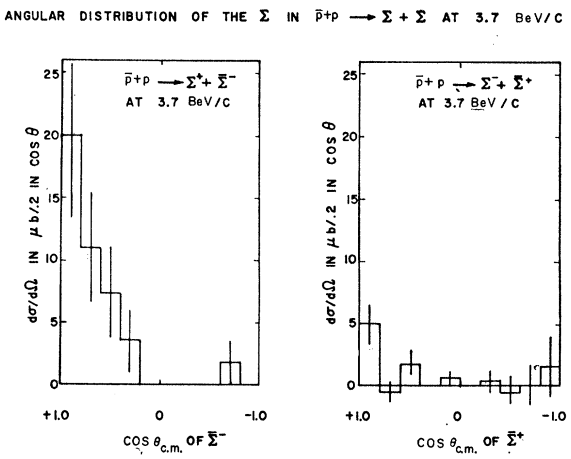

FIG. 7. Angular distributions of the $\bar{\Sigma}$ in the $\bar{p}p$ center-of-mass system in the reactions $\bar{p}+p \rightarrow \Sigma^++\bar{\Sigma}^-$ and $\bar{p}+p \rightarrow \Sigma^-+\bar{\Sigma}^+$.

[17] B. Musgrave, G. Petmezas, L. Riddiford, R. Bock, E. Fett, B. French, J. Kinson, Ch. Peyrou, M. Szeptycka, J. Badier, M. Bazin, L. Blaskovic, B. Equer, S. R. Borenstein, S. J. Goldsack, P. E. Grieve, D. H. Miller, J. Meyer, D. Revel, B. Tallini, and S. Zylberajch, *Proceedings of the Sienna International Conference on Elementary Particles, 1963* (Società Italiana di Fisica, Bologna, 1963), p. 301.

[18] H. Goldberg, S. Nussinov, and G. Yekutieli, Nuovo Cimento **28**, 446 (1963).

[19] K. Tanaka, Phys. Rev. **135**, B1186 (1964).

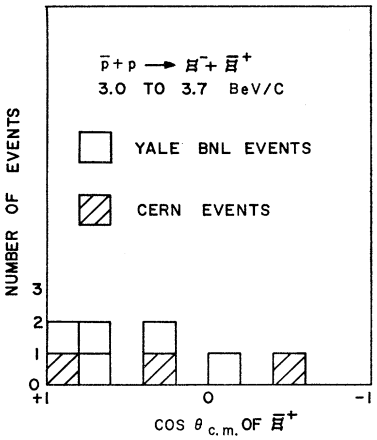

FIG. 8. Angular distribution of the $\bar{\Xi}^+$ in the $\bar{p}p$ center-of-mass system in the reaction $\bar{p}+p \rightarrow \Xi^-+\bar{\Xi}^+$.

VI. THREE- AND FOUR-BODY FINAL STATES

The $\bar{p}-p$ interactions leading to three- and four-body final states which include a hyperon, an antihyperon, and one or two pions, are dominated by hyperon isobar production. The final states studied in detail were

$$\bar{p}+p \rightarrow \Lambda+\bar{\Sigma}^{\pm}+\pi^{\mp} \text{ and charge conj.} \quad (6a)$$

$$\Lambda+\bar{p}+K^+ \text{ and charge conj.} \quad (6b)$$

$$\Xi^-+\bar{\Xi}^0+\pi^+ \text{ and charge conj.} \quad (6c)$$

$$\Lambda+\bar{\Lambda}+\pi^++\pi^-. \quad (6d)$$

Of particular interest are the productions which proceed through two-body intermediate states. The cross sections for such processes are listed in Table VI. These cross sections have been corrected for decay modes not observed in the present experiment, using the currently accepted values[20] of the various Y^* decay branching ratios.

A. The $\pi\Lambda\Sigma$ Final States

The events in this final state were divided into two groups

$$\bar{p}+p \rightarrow \Sigma^++\bar{\Lambda}+\pi^- \text{ or } \bar{\Sigma}^-+\Lambda+\pi^+ \quad (7a)$$

$$\rightarrow \Sigma^-+\bar{\Lambda}+\pi^+ \text{ or } \bar{\Sigma}^++\Lambda+\pi^-. \quad (7b)$$

Reaction (7a) occurred approximately three times as frequently as reaction (7b). The Dalitz plot obtained by plotting the square of the $\Sigma^{\pm}\pi^{\mp}$ or $\bar{\Sigma}^{\pm}\pi^{\mp}$ invariant masses versus the square of the $\Lambda\pi^{\pm}$ or $\bar{\Lambda}\pi^{\pm}$ masses, with the corresponding mass projections, is shown in Fig. 9. The production of the $Y_1^*(1385)$, the $Y_0^*(1405)$, and the $Y_0^*(1520)$, and their charge conjugate states, is clearly visible. A multi-parameter maximum likelihood fit was made to the $\Lambda\pi$ and $\Sigma\pi$ masses in these events to determine the relative amounts to isobar production. The following values were obtained, after appropriate detection efficiency corrections were made:

$$\bar{p}+p \rightarrow \bar{\Sigma}^{\pm}+Y_1^{*\mp}(1385) \text{ and c.c.} \quad 40\pm8\%$$
$$Y_1^{*\mp} \rightarrow \Lambda+\pi^{\mp} \text{ and c.c.}$$
$$\bar{p}+p \rightarrow \bar{\Lambda}+Y_0^*(1405) \text{ and c.c.} \quad 21\pm6\%$$
$$Y_0^* \rightarrow \Sigma^{\pm}+\pi^{\mp} \text{ and c.c.}$$
$$\bar{p}+p \rightarrow \bar{\Lambda}+Y_0^*(1520) \text{ and c.c.} \quad 14\pm6\%$$
$$Y_0^* \rightarrow \Sigma^{\pm}\pi^{\mp} \text{ and c.c.}$$
$$\bar{p}+p \rightarrow \bar{\Lambda}+\Sigma^{\pm}+\pi^{\mp} \text{ and c.c.} \quad 25\%.$$

TABLE V. Comparison of the octet exchange model of *SU3* with experiment from the reactions $\bar{p}+p \rightarrow \bar{Y}+Y$.

Reaction	Relative rate 8*A* (*F*)	Relative rate 8*s* (*D*)	Cross section (in μb) at 3.7 BeV/*c*
$\bar{p}+p \rightarrow \bar{\Lambda}+\Lambda$	9	1	82±8
$\bar{\Sigma}^0+\Sigma^0$	1	9	<26[a]
$\bar{\Lambda}+\Sigma^0$	3	3	35±5
$\bar{\Sigma}^0+\Lambda$	3	3	35±5
$\bar{\Sigma}^-\Sigma^+$	4	36	44±9

[a] This limit is deduced from charge independence using the cross section from $\bar{p}+p \rightarrow \Sigma^++\bar{\Sigma}^-$ and $\bar{p}+p \rightarrow \Sigma^-+\bar{\Sigma}^+$.

[20] M. Roos, Rev. Mod. Phys. **35**, 314 (1963).

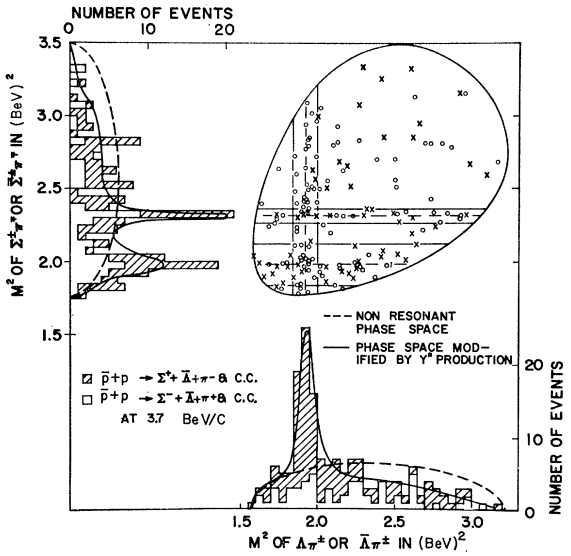

FIG. 9. Dalitz plot of the squares of the effective masses of $\Sigma\pi$ or $\bar{\Sigma}\pi$ versus the squares of the effective masses of $\Lambda\pi$ and $\bar{\Lambda}\pi$ in the reaction $\bar{p}+p \rightarrow \Sigma^{\pm}+\bar{\Lambda}+\pi^{\mp}$ or $\bar{\Sigma}^{\mp}+\Lambda+\pi^{\pm}$. The bands on the Dalitz plot represent the regions of the $Y_1^*(1385)$, the $Y_0^*(1405)$, and the $Y_0^*(1520)$. The dashed line on the mass projections represent Lorentz invariant phase space; the solid curves represent the fits to Y^* production discussed in the text.

TABLE VI. Production cross sections for two-body intermediate states involving hyperon isobars.

Intermediate state	Cross sections (μb)
$\Lambda^0+\bar{Y}_0^*(1405)$ plus charge conj.	28±10
$\Lambda^0+\bar{Y}_0^*(1520)$ plus charge conj.	37±18
$\Sigma^++\bar{Y}_1^{*-}(1385)$ plus charge conj.	36±11
$\Sigma^-+\bar{Y}_1^{*+}(1385)$ plus charge conj.	≤9
$Y_1^{*+}(1385)+\bar{Y}_1^{*-}(1385)$ plus charge conj.	5± 2
$Y_1^{*-}(1385)+\bar{Y}_1^{*+}(1385)$ plus charge conj.	8± 3
$\bar{\Xi}^0+\bar{\Xi}^{*0}(1530)$ plus charge conj.	2± 1

The solid curves superimposed on the mass projections in Fig. 9 correspond to this fit. In the above maximum likelihood fit, the masses and widths of the $Y_0^*(1405)$ and $Y_0^*(1520)$ were taken to have the currently accepted values.[20] The position and the width of the $Y_1^*(1385)$, however, were allowed to vary as free parameters. Their best values were:

$$M(Y_1^*)=1389\pm3 \text{ MeV},$$
$$\Gamma(Y_1^*)=26\pm5 \text{ MeV}.$$

This value of the width is significantly smaller than the usually quoted value of $\Gamma=50$ MeV.[20] There are a number of other experiments[21–23] in which narrow widths, consistent with this experiment, were obtained. It is also possible, however, that strong interference effects in these complicated reactions are responsible for the apparently reduced width.

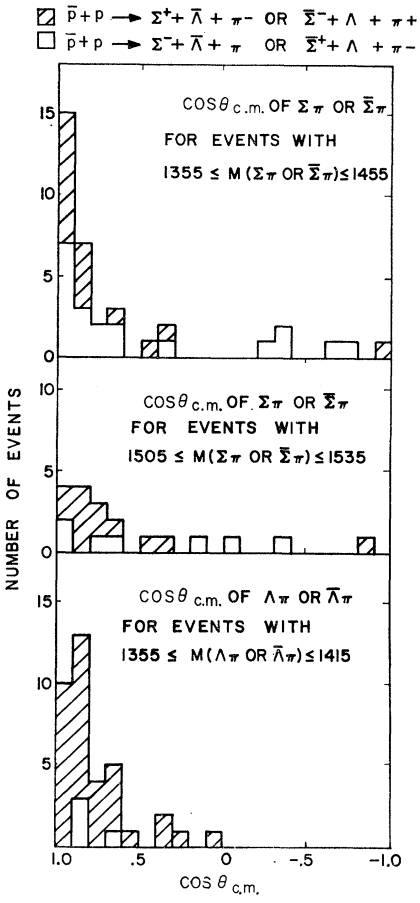

FIG. 10. Angular distributions in the $\bar{p}p$ center-of-mass system for the Y^* or $\bar{Y}^*$ produced in the reactions $\bar{p}+p\rightarrow\Sigma^{\pm}+\bar{\Lambda}+\pi^{\mp}$ or $\bar{\Sigma}+\Lambda+\pi^{\pm}$. The Y^* angle is taken with respect to the incident proton, and the $\bar{Y}^*$ angles are with respect to the antiprotons. The top graph is the region of the $Y_0^*(1405)$, the middle graph is for the $Y_0^*(1520)$, and the bottom graph is for the $Y_1^*(1385)$.

[21] M. Alston and M. Ferro-Luzzi, Rev. Mod. Phys. 33, 416 (1961).
[22] R. K. Adair, Rev. Mod. Phys. 33, 406 (1961).
[23] H. Foelsche and H. Kraybill (private communication).

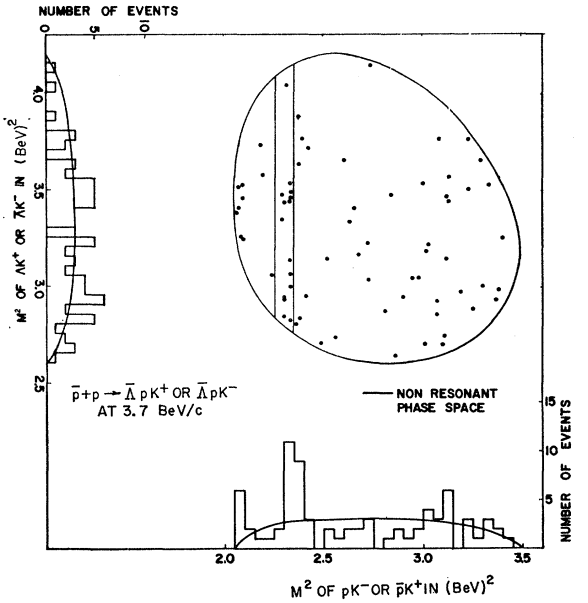

FIG. 11. Dalitz plot for the squares of the effective masses of the ΛK^+ or $\bar{\Lambda}K^-$ combinations versus the pK^- or $\bar{p}K^+$ combinations in the reactions $\bar{p}+p\rightarrow\Lambda+\bar{p}+K^+$ or $\bar{\Lambda}+p+K^-$. The band on the Dalitz plot represents the region of the $Y_0^*(1520)$.

The production angular distributions for $Y_0^*(1405)$, $Y_0^*(1520)$, and $Y_1^*(1385)$, respectively, from top to bottom, are shown in Fig. 10. Here the angles of the Y^* are taken with respect to the proton direction and the $\bar{Y}^*$ with respect to the incident $\bar{p}$ direction, in the $\bar{p}p$ center-of-mass system. All three distributions show strong forward peaking. It may be interesting to note that this peaking becomes stronger as the energy available above the threshold for the process increases. The angular distribution of the pions shows no strong deviations from isotropy.

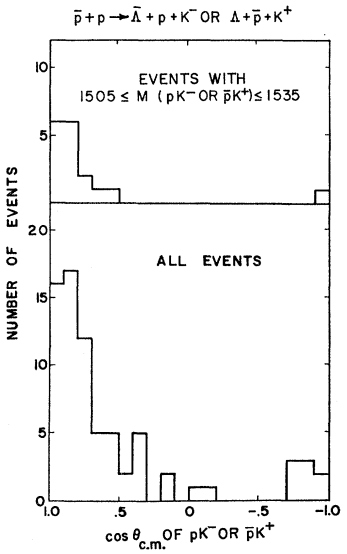

FIG. 12. Angular distribution of the pK^- or $\bar{p}K^+$ combinations in the $\bar{p}p$ center-of-mass system in the reactions $\bar{p}+p\rightarrow\Lambda+\bar{p}+K^+$ or $\bar{\Lambda}+p+K^-$. The angles of the $\bar{p}K^+$ combination are taken with respect to the incident $\bar{p}$, and the pK^- is taken with respect to the incident proton. In the top graph those events are selected in which the pK^- or $\bar{p}K^+$ effective mass is in the $Y_0^*(1520)$ region.

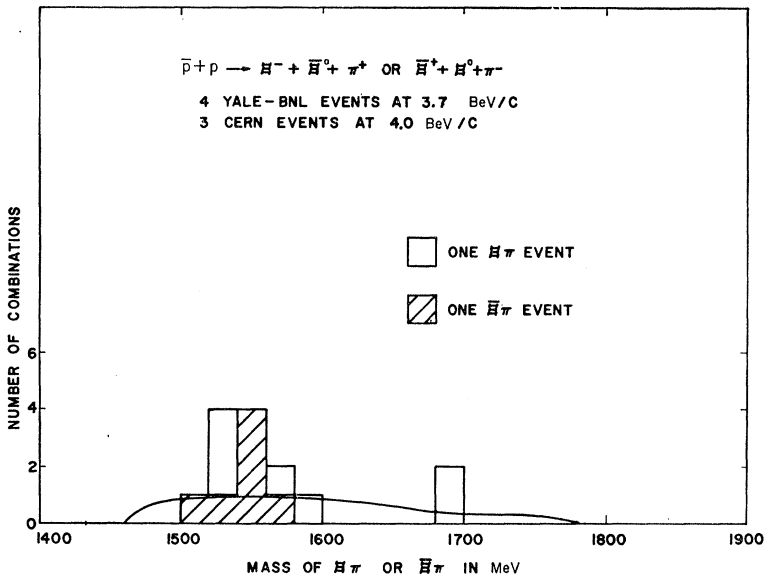

FIG. 13. Distribution of the effective masses of the $\Xi^-\pi^+$, $\bar{\Xi}^+\pi^-$, $\Xi^0\pi^-$, and $\bar{\Xi}^0\pi^+$ combinations in the reactions $\bar{p}+p \rightarrow \Xi^-+\bar{\Xi}^0+\pi^+$ or $\bar{\Xi}^+ +\Xi^0+\pi^-$. There are two mass combinations per event in this distribution. The solid curve represents phase space.

The forward peaking of the Y^* production angular distributions suggests a single-particle-exchange mechanism in these reactions. This is further borne out by the fact that the production of $\Sigma^-+\bar{Y}^{*+}(1385)$ or c.c., which requires a net charge exchange of two, is strongly depressed with respect to $\Sigma^+ + \bar{Y}^{*-}(1385)$ and c.c. production.[24]

B. The $\Lambda\bar{p}K^+$ or $\bar{\Lambda}pK^-$ Final State

The Dalitz plot which results when the square of the ΛK^+ or $\bar{\Lambda}K^-$ mass is plotted against the square of the $\bar{p}K^+$ or pK^- mass is shown in Fig. 11. The enhancement in the $\bar{p}K^+$ or pK^- mass near 1520 MeV indicates the presence of $\Lambda+\bar{Y}_0^*(1520)$ and $\bar{\Lambda}+Y_0^*(1520)$ production, with subsequent decay of the Y_0^* into p^+K^- and $\bar{Y}_0^*$ into $\bar{p}+K^+$. Comparison of the rate for this process with those for $\Lambda+\bar{Y}_0^*(1520)$ and $\bar{\Lambda}+Y_0^*(1520)$, where $Y_0^* \rightarrow \Sigma^\pm+\pi^\mp$ and $\bar{Y}_0^* \rightarrow \bar{\Sigma}^\pm+\pi^\mp$, as observed in the $\Lambda\Sigma\pi$ final states, yields a branching ratio for the $Y_0^*(1520)$ decay which is consistent with the usually accepted value.[20]

In addition to the enhancement near 1520 MeV in the $\bar{p}K^+$ or pK^- mass spectrum, there seems to be an enhancement at the low end of the $\bar{p}K^+$ or pK^- mass spectrum: 6 events are observed where phase space predicts one (see Fig. 11). This effect might be associated with the s-wave $\bar{K}p$ interaction studied by Humphrey and Ross.[25]

Figure 12 shows that the antibaryons are emitted in the forward direction, as in other final states.

C. The $\Xi^-\bar{\Xi}^0\pi^+$ or $\bar{\Xi}^+\Xi^0\pi^-$ Final State

Four events of this type were observed in the present experiment. In two events the $\bar{\Xi}^0$'s were unambiguously identified by their decay into $\bar{\Lambda}^0$'s which in turn decayed into antiprotons.[7] Three of these final states have also been observed in $\bar{p}-p$ interactions at 4.0 BeV/c at CERN.[26] Data from these seven events have been combined; the distribution of the $\Xi\pi$ or $\bar{\Xi}\pi$ effective masses is shown in Fig. 13. Each event contributes two masses in this distribution: $\Xi^-\pi^+$ and $\bar{\Xi}^0\pi^+$, or $\bar{\Xi}^+\pi^-$ and $\Xi^0\pi^-$. The concentration of masses in the region between 1520 and 1560 MeV suggests the production of the $\Xi^*(1530)$; the data are consistent with 100% production of this isobar.

D. The $\Lambda\Lambda\pi^+\pi^-$ Final State

The reactions $\bar{p}+p \rightarrow \Lambda+\bar{\Lambda}+\pi^+ +\pi^-$ are dominated by the formation of the $Y_1^*(1385)$ and its charge conjugate state.[27] The $\Lambda\pi^+\pi^-$ and $\bar{\Lambda}\pi^+\pi^-$ mass spectra show no statistically significant structure, although some formation of the $Y_0^*(1520)$ might be present. There is no resonance structure in the $\pi^+\pi^-$ mass spectrum.

The combined $\Lambda\pi^\pm$ and $\bar{\Lambda}\pi^\pm$ mass spectra from this reaction are shown on the left in Fig. 14. There are four possible mass combinations from each event in this distribution, but a maximum of two isobars can be produced per event. Considering this background, it was esti-

[24] See also C. Baltay, J. Sandweiss, H. D. Taft, B. B. Culwick, W. B. Fowler, J. K. Kopp, R. I. Louttit, J. R. Sanford, R. P. Shutt, D. L. Stonehill, A. M. Thorndike, and M. S. Webster, Phys. Rev. Letters **11**, 346 (1963).

[25] For a discussion of this phenomenon, with a complete set of references, see R. H. Dalitz, *Strange Particles and Strong Interactions* (Oxford University Press, New York, 1962), Chap. VII.

[26] B. Musgrave, G. Petmezas, L. Riddiford, R. Bock, E. Fett, B. R. French, J. B. Kinson, Ch. Peyrou, M. Szeptycka, J. Badier, M. Bazin, B. Equer, J. Huc, S. Borenstein, S. J. Goldsack, D. H. Miller, S. Misbahuddin, J. Meyer, D. Revel, B. Tallini, and S. Zylberajch, Ref. 17, p. 312.

[27] Preliminary results on this final state were published previously: C. Baltay, J. Sandweiss, H. D. Taft, B. B. Culwick, W. B. Fowler, J. K. Kopp, R. I. Louttit, J. R. Sanford, R. P. Shutt, A. M. Thorndike, and M. S. Webster, Phys. Rev. Letters **11**, 32 (1963).

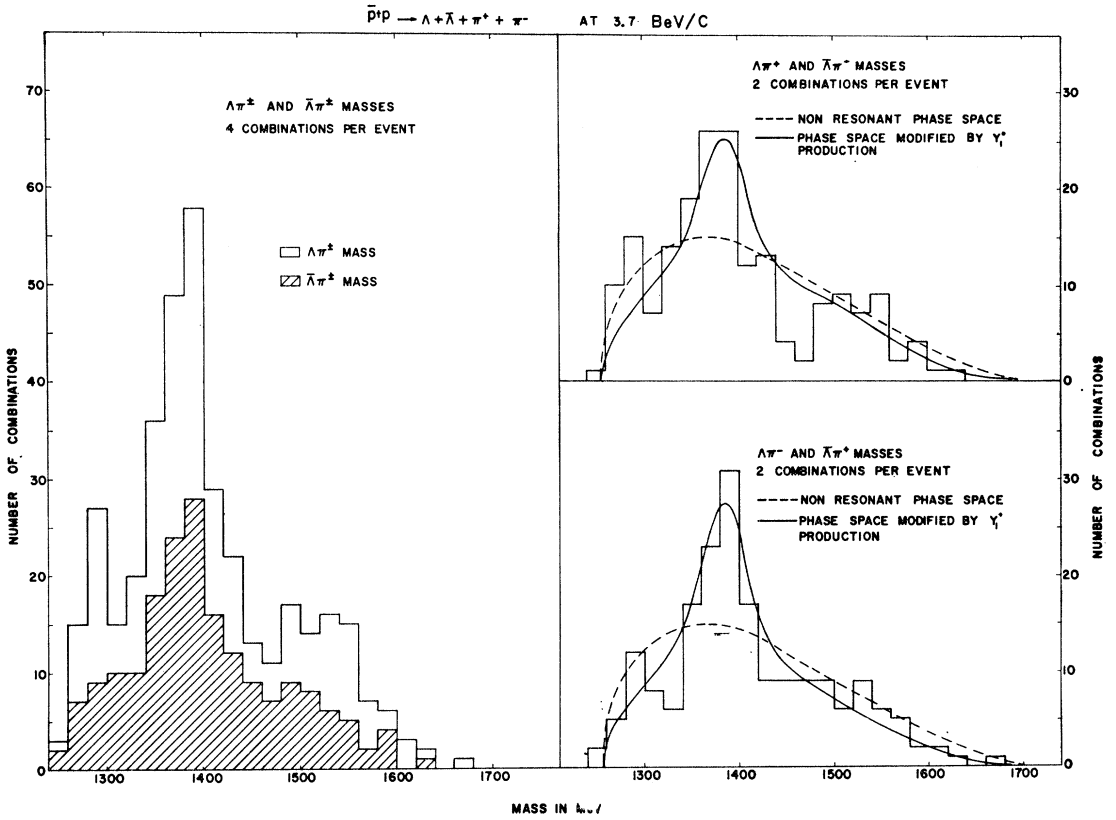

FIG. 14. Distributions in the $\Lambda\pi^\pm$ and $\bar{\Lambda}\pi^\pm$ effective masses in the reaction $\bar{p}+p \rightarrow \Lambda+\bar{\Lambda}+\pi^+ +\pi^-$. On the left, there are four mass combinations per event; the $\bar{\Lambda}\pi^\pm$ masses are cross-hatched. On the right, the distribution has been separated into $\Lambda\pi^+$ or $\bar{\Lambda}\pi^-$ masses, the possible decay products of $Y_1^{*+}(1385)$ or $\bar{Y}_1^{*-}(1385)$ (top), and $\Lambda\pi^-$ or $\bar{\Lambda}\pi^+$ masses, the possible decay products of $Y_1^{*-}(1385)$ or $\bar{Y}_1^{*+}(1385)$ (bottom). The solid curves represent the fit to hyperon isobar production rates given in Table VII.

mated that a Y_1^* or a $\bar{Y}_1^*$ or both were produced in 80% of the events. To study the importance of the production of Y_1^{*+} or its antistate relative to the production of Y_1^{*-} or its antistate, the $\Lambda\pi^+$ or $\bar{\Lambda}\pi^-$ masses were separated from the $\Lambda\pi^-$ or $\bar{\Lambda}\pi^+$ masses. The resulting two distributions are shown on the right-hand side of Fig. 14, and indicate that the $Y_1^{*-}(\bar{Y}_1^{*+})$ are produced at least as strongly as the $Y_1^{*+}(\bar{Y}_1^{*-})$. Evidence for $Y_1^*+\bar{Y}_1^*$ pair production is shown in Fig. 15. The upper half is a scattergram of the $\bar{\Lambda}\pi^-$ mass versus the $\Lambda\pi^+$ mass, folded around the 45° line of charge conjugation symmetry. The lower half is the same for the $\bar{\Lambda}\pi^+$ mass versus the $\Lambda\pi^-$ mass.

TABLE VII. Relative production rates for processes leading to the final state $+\Lambda+\bar{\Lambda}\pi^+ +\pi^-$.

	Process	Fractoin
(a)	$\bar{p}+p \rightarrow Y_1^{*+}+\bar{Y}_1^{*-}$	0.20
(b)	$\rightarrow Y_1^{*-}+\bar{Y}_1^{*+}$	0.30
(c)	$\rightarrow Y_1^{*+}+\bar{\Lambda}+\pi^-$ and c.c.	0.20
(d)	$\rightarrow Y_1^{*-}+\bar{\Lambda}+\pi^+$ and c.c.	0.10
(e)	$\rightarrow \Lambda+\bar{\Lambda}+\pi^+ +\pi^-$	0.20

The results of a χ^2 analysis of the relative frequency of processes leading to the $\Lambda+\bar{\Lambda}+\pi^+ +\pi^-$ final state are presented in Table VII. The rates of processes a, b, c, and d listed in the table were used as the four independent parameters in the χ^2 analysis. The mass and width of the Y_1^* were held fixed at $E_0=1385$ MeV and $\Gamma=50$ MeV. The known experimental mass resolution was folded in. Echo effects, like for example the effect of the production of Y_1^{*+}, decaying into $\Lambda^0+\pi^+$, on the $\Lambda\pi^-$ and $\bar{\Lambda}\pi^+$ mass spectra, were estimated by Monte Carlo programs and were taken into consideration in the χ^2 analysis. Errors on the rates given in Table VI were not explicitly calculated but are of the order of ± 0.10.

In contrast with the other two-body intermediate or final state processes in $\bar{p}+p$ collisions, the production of Y_1^* pairs does not seem to be dominated by a simple single-particle-exchange mechanism: because of the absence of a strongly coupled, doubly charged $B=0$, $S=\pm 1$ state, the production of $Y_1^{*-}+\bar{Y}_1^{*+}$ pairs should be strongly depressed relative to the production of $Y_1^{*+}+\bar{Y}_1^{*-}$ pairs. The data indicate that this is not the case; $Y_1^{*-}+\bar{Y}_1^{*+}$ production is at least as strong or stronger than $Y_1^{*+}+\bar{Y}_1^{*-}$ production. A possible ex-

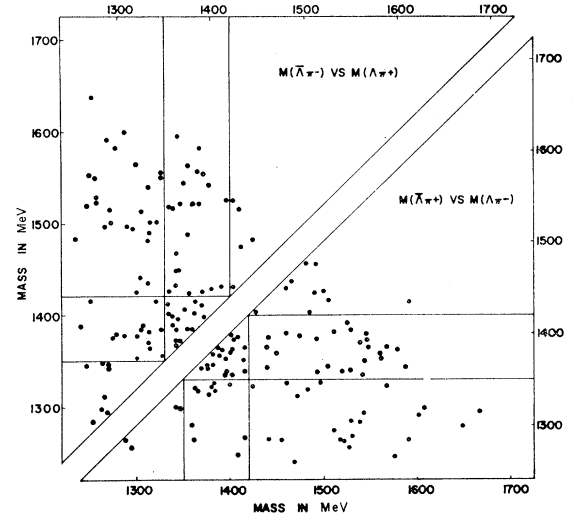

FIG. 15. Scattergrams of the $\bar{\Lambda}\pi^-$ mass versus the $\Lambda\pi^+$ mass (top) and the $\bar{\Lambda}\pi^+$ mass versus the $\Lambda\pi^-$ mass (bottom). Both scattergrams have been folded around the 45° line of charge conjugation symmetry.

planation of this absence of single-particle exchange is the fact that the available energy in these $\bar{p}p$ collisions is less than 200 MeV above the Y_1^* pair production threshold. The angular distribution of the $\bar{\Lambda}\pi$ combinations in the $\Lambda+\bar{\Lambda}+\pi^++\pi^-$ final states is shown in Fig. 16. The forward peaking here is not nearly as strong

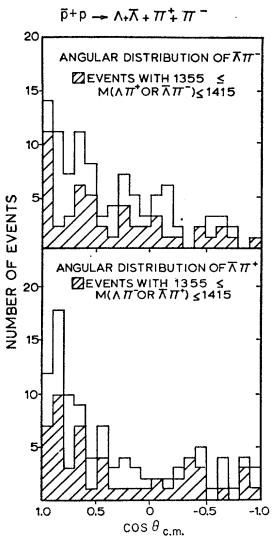

FIG. 16. Angular distribution of the $\bar{\Lambda}\pi^-$ and $\bar{\Lambda}\pi^+$ combinations with respect to the incident $\bar{p}$ direction in the $\bar{p}p$ center-of-mass system in the reaction $\bar{p}+p\rightarrow\Lambda+\bar{\Lambda}+\pi^++\pi^-$. In the distribution on top, events with $\Lambda\pi^+$ or $\bar{\Lambda}\pi^-$ masses in the $Y_1^{*+}(1385)$ or $\bar{Y}_1^{*-}$ (1385) regions are crosshatched. In the distribution on the bottom the same has been done for events with $\Lambda\pi^-$ or $\bar{\Lambda}\pi^+$ masses in the Y_1^{*-} or $\bar{Y}_1^{*+}$ regions.

as in the other two-body processes, where single-particle exchange seems more dominant.

E. Comparison with $p+p$ Reactions

Hyperon production was studied in $p-p$ collisions at an incident proton momentum of 3.6 BeV/c,[28] almost identical to the incident $\bar{p}$ momentum of this experiment. Some reactions in the $p-p$ collisions are the same as in the $\bar{p}-p$ collisions if the p is replaced by $\bar{p}$ in both the initial and final states. These reactions, along with their observed cross sections, are listed below for comparison:

$$\begin{aligned}
p+p &\rightarrow \Lambda^0+K^++p, && \sigma=51\pm12\ \mu\text{b}\\
&\rightarrow \Sigma^0+K^++p, && \sigma=13\pm\ 7\ \mu\text{b}\\
&\rightarrow \Sigma^++K^0+p, && \sigma=30\pm10\ \mu\text{b}\\
p+\bar{p} &\rightarrow \Lambda^0+K^++\bar{p}\text{ and c.c.}, && \sigma=29\pm\ 5\ \mu\text{b}\\
&\rightarrow \Sigma^0+K^++\bar{p}\text{ and c.c.}, && \sigma=13\pm\ 4\ \mu\text{b}\\
&\rightarrow \Sigma^++K^0+\bar{p}\text{ and c.c.}, && \sigma=14\pm\ 4\ \mu\text{b}.
\end{aligned}$$

It is perhaps surprising that the cross sections for these reactions are lower in $\bar{p}-p$ reactions, since the simplest single-particle- (π, K or K^*) exchange diagrams predict that these reactions proceed more strongly in $\bar{p}-p$ reactions. A possible explanation for this fact is that absorption processes are much stronger and damp the associated production channels more severely in $\bar{p}-p$ reactions than in $p-p$ reactions.

ACKNOWLEDGMENTS

We wish to thank all of the numerous people whose efforts made this experiment possible. The exposure would have been impossible without the unfailing support of the BNL AGS staff and the 20-in. HBC operating crews. The scanning and measuring staffs associated with the BNL Bubble Chamber Group and the Yale High Energy Physics Group carried the burden of the data reduction. The Yale authors would like to express their gratitude for the hospitality they received from both the AGS Department and the Bubble Chamber Group during their many stays at Brookhaven in connection with this experiment. Finally, it is a pleasure to acknowledge the help of H. Brown, W. Fowler, T. Ludlam, J. Sanford, P. Slattery, and D. Stonehill who have collaborated in various stages of the experiment.

[28] R. I. Louttit, T. W. Morris, D. C. Rahm, R. R. Rau, A. M. Thorndike, W. J. Willis, and R. M. Lea, Phys. Rev. **123**, 1465 (1961).